

Origami-based Spintronics

A. T. Costa*

Instituto de Física, Universidade Federal Fluminense, 24210-346 Niterói, RJ, Brazil

M. S. Ferreira†

School of Physics and CRANN, Trinity College Dublin, Dublin 2, Ireland

A. H. Castro Neto

*Graphene Research Centre and Department of Physics,
National University of Singapore, 6 Science Drive 2, 117546, Singapore and*

*Department of Physics, Boston University,
590 Commonwealth Ave., Boston, MA, 02215, USA*

(Dated: April 11, 2013)

Abstract

We show that periodically folded graphene sheets with enhanced spin-orbit interaction due to curvature effects can carry spin polarized currents and have gaps in the electronic spectrum in the presence of weak magnetic fields. Our results indicate that such origami-like structures can be used efficiently in spintronic applications.

PACS numbers:

*Electronic address: antc@if.uff.br

†Electronic address: ferreirm@tcd.ie

Often hailed as a wonder material due to its impressive physical properties [1], graphene has opened several venues of basic science exploration and it is a material that has a tremendous technological potential. Despite its potential applicability, the lack of a bandgap is a well known limitation that currently prevents the use of graphene in digital electronic applications [2]. Different strategies have been attempted to remedy this shortcoming, namely, by quantum confinement in the form of nanoribbons and quantum dots [3, 4], by stacking graphene sheets in bilayers in the presence of a perpendicular electric field [5, 6], by strain-engineering its electronic structure [7–9], or by simply chemically doping the graphene sheets [10, 11]. Unfortunately, these attempts have so far failed to produce technologically relevant semiconducting graphene due to several difficulties that go from the small size of the gaps they produce to the disorder that they introduce.

On a different front, the field of spintronics appears as one of the most promising areas for graphene since the extremely small spin-orbit interaction (SOI) of carbon makes the spin dissipation that otherwise exists in most materials practically negligible [12, 13]. This suggests that whatever information is stored in the electronic spin of graphene can be retained for times considerably longer than those found in ordinary metals. Furthermore, this information can travel much longer distances with very little loss [14–16]. Not surprisingly, there is a growing interest in graphene-based spintronics as demonstrated by the volume of recent literature on the topic [17].

Driven by the necessity of a bandgap and by the growing interest in graphene-based spintronics, in this letter we propose a simple mechanism that not only produces a gapped electronic structure in graphene but that also spin-polarizes its current. We show that this effect arises quite simply by the combined presence of two key ingredients: the SOI and an externally applied magnetic field. While magnetic fields are controllable, the SOI of a material is normally constant and small in the case of carbon. Therefore, it might seem too ambitious to amplify both ingredients enough for the appearance of a possible gap. Nevertheless, recent discoveries have demonstrated that the SOI is enhanced when graphene is mechanically bent away from its planar geometry [18–21] suggesting that folding might function as a viable mechanism to induce a bandgap. In fact, here we show that folded graphene sheets in the presence of externally applied magnetic fields may display both a gapped electronic structure and spin-polarized currents. Not being possible to fold 3-dimensional structures, this possibility was never imagined with bulk materials but paves

the way to a whole new approach of dealing with spin electronics in 2-dimensional systems, giving rise to the so-called origami spintronics.

It is convenient to start by showing that the two aforementioned key ingredients indeed lead to a bandgap in graphene. Let us then consider a graphene sheet with SOI and in the presence of an externally applied magnetic field. For energies close to the Dirac point, the band Hamiltonian H is commonly described by a 2-dimensional Dirac equation. In this case, the Hamiltonian is given by [22]: $\hat{H} = v_F \hat{1} \otimes \vec{\sigma} \cdot \vec{p} + 2\lambda(\sigma_x \otimes \tau_y + \sigma_y \otimes \tau_x) + \gamma \hat{1} \otimes \tau_z$, where v_F is the Fermi velocity, $\sigma_{x,y,z}$ are Pauli matrices acting on the sublattice space, $\tau_{x,y,z}$ are Pauli matrices acting on the spin subspace, $\vec{p} = -i\hbar\vec{\nabla}$ is the momentum operator, λ represents the strength of the SOI and γ is the Zeeman-field factor. Note that the Hamiltonian recovers the standard form for pristine graphene when both γ and λ vanish, so it is convenient to express the Hamiltonian $\hat{H} = \hat{H}_0 + \hat{V}$, where \hat{H}_0 is the pristine Hamiltonian and \hat{V} accounts for the γ - and λ -dependent perturbation. When expressed on the basis formed by the vector $\Psi = (\psi_a^\uparrow, \psi_a^\downarrow, \psi_b^\uparrow, \psi_b^\downarrow)^T$, where ψ_ζ^σ is the electron wavefunction on sublattice ζ with spin σ , the Hamiltonian is written in matrix form as:

$$H(k_x, k_y) = \begin{pmatrix} -\gamma & 0 & k_x + ik_y & -2i\lambda \\ 0 & \gamma & 0 & k_x + ik_y \\ k_x - ik_y & 0 & -\gamma & 0 \\ 2i\lambda & k_x - ik_y & 0 & \gamma \end{pmatrix} \quad (1)$$

The four corresponding eigenvalues are:

$$E(k) = \pm \sqrt{k^2 + \gamma^2 + 2\lambda^2 \pm 2\sqrt{\lambda^4 + k^2(\gamma^2 + \lambda^2)}}, \quad (2)$$

where $k^2 = k_x^2 + k_y^2$. Figure 1(a) shows the dispersion $E(k)$ for arbitrary values of λ and γ . Note the distinctive energy gap $\Delta = \frac{2\lambda}{\sqrt{1+(\lambda/\gamma)^2}}$ around $E = 0$. The characteristic linear dispersion relation of pristine graphene reappears from Eq. (2) when $\gamma = \lambda = 0$. It is worth pointing out that either γ or λ alone is not capable to induce the bandgap opening, as shown in Figs. 1(b) and 1(c). Only when both quantities are non-zero, will the bandgap appear. This is explained by the fact that γ and λ define two complementary energy scales and the magnitude of the bandgap Δ is determined ultimately by the smallest of these two quantities.

Let us now consider folding the graphene sheet as a SOI-enhancing mechanism. In this case, however, the SOI is not homogeneously distributed but spatially limited to the region

of the graphene sheet surrounding the non-planar deformations. We consider a corrugated structure where curved deformations to the graphene sheet are ordered in a periodic structure. This can be achieved by patterning a substrate in the form of periodic trenches [25] on top of which a graphene sheet is deposited. In this way, the graphene sheet alternates between curved and flat regions, the dimensions of which will depend on the geometry of the patterned substrate. Figure 2(a) shows an image of a typical corrugated sheet composed of a sequence of parallel ridges and troughs. While the diagram depicts a sheet of width L , it is supposed to represent a system where $L \gg S$, meaning that for practical purposes $L \rightarrow \infty$. For the sake of simplicity, we consider the corrugated graphene sheet made of a series of curved regions, all composed of semi-circular cross sections with curvature radius R , equally spaced by a distance D , the cross section of which is schematically shown in Fig. 2b. It is worth noting that this setup is equivalent to an array of half nanotubes joined seamlessly together by flat nanoribbons. Since the material has to comply during folding, this kind of distortion of the graphene sheet does not introduce the disorder that is so deleterious to the transport properties in other gap-opening proposals.

Differently from the previous case where we looked at how the electronic band structure changes with the inclusion of the SOI plus the Zeeman term across the entire system, in the corrugated case we investigate how the conductance of the material responds to the addition of exactly the same ingredients, now in a periodic arrangement as shown in Fig. 2b. In this case both these ingredients are added to the pristine Hamiltonian only where the graphene sheet has a non-zero curvature. The advantage of studying the transport response of the system is that we are able not only to identify the opening of a bandgap, which appears as a region of zero conductance, but we can simultaneously investigate the spin dependence of the transport response when the conductance is finite. In this way, we can study the appearance of a bandgap and assess its potential impact on spintronics applications at the same time.

Rather than using the Dirac equation to describe the electronic structure of the system, we consider the tight-binding (TB) Hamiltonian whose accuracy is not limited to a narrow energy range surrounding the Dirac point [26]. The Hamiltonian is written as $\hat{H} = \sum \hat{a}_{j,\sigma} \hat{b}_{j',\sigma} + \hat{V}$, where the operators $\hat{a}_{j,\sigma}^\dagger$ ($\hat{a}_{j,\sigma}$) creates (annihilates) an electron at site j and spin σ on the sublattice A. The $\hat{b}_{j,\sigma}^\dagger$ and $\hat{b}_{j,\sigma}$ are the corresponding operators for the B sublattice. The operator $\hat{V} = i\lambda \sum_{ll'} \sum_{\alpha\beta} \hat{z} \cdot (\vec{\sigma}_{\alpha\beta} \times \vec{d}_{ll'}) c_{l\alpha}^\dagger c_{l'\beta} - \gamma \sum_{l\alpha} \alpha c_{l\alpha}^\dagger c_{l\alpha}$ represents

the effects of a Rashba spin-orbit coupling [22] plus a Zeeman field. $\vec{d}_{l'}$ is the position of site l' relative to site l . $\vec{\sigma}$ is the vector formed by the Pauli matrices and the index α in the last sum takes the value +1 for majority spins and -1 for minority spins. The Rashba term arises whenever inversion symmetry in the direction perpendicular to the graphene sheet is broken, a condition realized for samples deposited on a substrate or in the presence of an electric field perpendicular to the sheet plane.

The parameters λ and γ are dependent on the curvature and on the applied magnetic field, respectively. The former can be estimated from References [12, 13], which studied the SOI in carbon nanotubes, and the latter can be extracted from characteristic values of magnetic fields. For the case shown in Fig. 2b the potential \hat{V} acts only where the curved regions are located. In other words, we must consider an infinite long sheet of graphene with an array of M equally spaced regions of width πR separated by a distance D . Following Refs. [12, 13], λ is inversely proportional to the radius R , which means that higher curvatures correspond to narrower curved sections with correspondingly stronger values for λ . In the extreme limit of very high curvatures ($R \rightarrow 0$) the width of the regions with non-zero SOI becomes small, giving rise to a geometry depicted by Fig. 2c. In all cases, we assume that the corrugated structure is connected by leads made of semi-infinite pristine graphene.

The conductance is calculated by the Kubo formula expressed in terms of the single particle Green function G , which in turn, is defined as $G(E) = (E \hat{1} - \hat{H})^{-1}$, where E is the energy and $\hat{1}$ is the identity operator. The zero bias DC conductance Γ is written as:

$$\Gamma = \frac{4e^2}{h} \text{ReTr} \left([\tilde{G}]_{00} t_{01} [\tilde{G}]_{11} t_{10} - t_{01} [\tilde{G}]_{10} t_{01} [\tilde{G}]_{10} \right) \quad (3)$$

Here, $\tilde{G}_{l\alpha, l'\beta} = [G_{l\alpha, l'\beta} - (G_{l'\beta, l\alpha})^*]/2i$ and $[G]_{AB}$ is the matrix formed by the Green function elements connecting unit cells A and B . α and β are spin indices. We define unit cells as lines along the “armchair” direction. The trace is taken over both site and spin indices. All Green functions in the above expression are evaluated at the Fermi level.

In Fig. 3 we show the results for the spin-dependent conductance as a function of the Fermi level E_F for $M = 10, 15$, and 50 . The first thing worth noticing is the opening of a gap as M increases, as shown in the inset of Fig. 3(a). The magnitude of the gap increases with M and tends to a saturation value when $M \gg 1$. In addition, outside the gapped energy region, the conductance becomes spin dependent, i.e., the transport properties for the \uparrow and \downarrow spin electrons become completely asymmetric, which is a basic requirement for

exploring the use of any material in spintronics. Such an asymmetry in the spin-dependent conductance means that these corrugated systems can function as spin polarizers for the electronic currents in graphene. The inset of Fig. 3(b) shows the spin-polarization of the current, defined as $I_{sp} = (I_{\uparrow} - I_{\downarrow}) / (I_{\uparrow} + I_{\downarrow})$, as a function of E_F whereas the inset of Fig. 3(c) depicts I_{sp} as a function of λ . Note the sign change of I_{sp} on either side of the band gap. This feature is seen in all our results.

Having carried out the numerical evaluation of Eq. (3) within the TB model and observed the appearance of the bandgap as well as the spin asymmetry in the conductance, it is instructive to assess the robustness and generality of these findings by using alternative methods. With that in mind, we introduce a simplified approach that is far less computationally involved and yet capable of capturing the contribution from the two key ingredients, namely the SOI and the Zeeman term. For the sake of simplicity, we investigate the limit $R \rightarrow 0$, shown schematically in Fig. 2(c). In this limit, the SOI-enhancing curvature becomes extremely large at the same time as the extension of the curved region becomes vanishingly small. The smooth undulations shown in Figs. 2(a) and 2(b) give way to equally spaced creases on the graphene sheet, ideally represented by Dirac delta functions that mark the locations where both the SOI and the Zeeman term are non-zero. Moreover, a further simplification is to assume electrons moving along the direction normal to the creases. The Hamiltonian in this case becomes $\hat{H} = \hat{H}_0 + \sum_{j=1}^M \hat{V} \delta(x - jD)$, where the operators \hat{H}_0 and \hat{V} have been previously defined, the only difference being that $k_y = 0$ and $k = k_x$. In other words, the problem in question is now solved by considering Dirac equation for massless particles under the action of a perturbing potential made of a series of λ - and γ -dependent delta functions.

Care must be taken when solving Dirac equation in the presence of delta function potentials because the wavefunctions become discontinuous in this case [27, 28]. The boundary condition needed to specify the wavefunctions on opposite sides of a given delta function at an arbitrary position, say $x = 0$, is given by $\Psi_+ = e^{\hat{A}} \Psi_-$, where $\hat{A} = -\hat{V}(\hat{H}_0)^{-1}$, Ψ_+ (Ψ_-) being the wavefunction on the right (left) hand side of the delta function position. So, for an array of M delta functions equally spaced by a distance D in between two leads, we write $\Psi_R = \hat{T} \Psi_L$, where Ψ_R (Ψ_L) is the wavefunction on the right (left) lead and \hat{T} is the transfer matrix.

The transfer matrix is written as $T = [\hat{L}(x_R)]^{-1} [e^{\hat{A}} \hat{S}(D)]^{M-1} \hat{L}(x_L)$, where:

$$\hat{L}(x) = \begin{pmatrix} e^{ikx} & 0 & -e^{-ikx} & 0 \\ 0 & e^{ikx} & 0 & -e^{-ikx} \\ e^{ikx} & 0 & e^{-ikx} & 0 \\ 0 & e^{ikx} & 0 & e^{-ikx} \end{pmatrix} \quad (4)$$

and

$$\hat{S}(x) = \begin{pmatrix} \cos kx & 0 & i \sin kx & 0 \\ 0 & \cos kx & 0 & i \sin kx \\ i \sin kx & 0 & \cos kx & 0 \\ 0 & i \sin kx & 0 & \cos kx \end{pmatrix}. \quad (5)$$

x_L and x_R are the positions marking the start of the left and right leads, respectively.

It is now straightforward to extract the spin-resolved transmission coefficient from the transfer matrix \hat{T} and plot it as a function of the energy, which is proportional to the wavevector k . Since the conductance is also proportional to the transmission coefficient, we can now compare the results of this simplified approach with the TB-based results. In Fig. 4 we show results for $M = 2$ delta functions a distance D apart calculated with the simplified approach as well as with the TB adapted for normal incidence. Quantitative agreement is not expected because the discrete delta function representation in the TB-model is fundamentally different from the continuous one. From a qualitative point of view, however, both methodologies lead to the appearance of a low-energy conductance gap followed by a spin-polarized current for energies outside the bandgap. This commonality found with two distinct methodologies is indicative of the robustness of our findings, which is further confirmed by recent calculations based on Density Functional Theory results also displaying bandgap features when the SOI is enhanced by curvature effects [29].

In addition to folding, adsorbants that deform the pristine planar structure of graphene sheets also function as SOI-enhancers. Therefore, it is possible to combine them both such that SOI-enhancing adsorbants might get attached to mechanically curved regions which themselves possess enhanced spin-orbit coupling. While we are not able to quantify the precise contributions coming from each one of the different mechanisms, curvature and dopants acting jointly together will certainly amplify the overall effect of spin-polarization of the charge currents as well as the bandgap in the electronic structure of the system.

In summary, we have shown that by adding the Zeeman term and the SOI to the Hamiltonian of pristine graphene, we force the opening of a bandgap in its electronic structure and induce its charge current to become spin polarized. Both additions to the Hamiltonian are experimentally feasible and are mimicked by an externally applied magnetic field and by deforming the graphene sheet out of its planar geometry through folding. With the increasing degree of experimental control on both the chemistry and the geometry of nanoscaled surfaces, it is possible that by engineering the shape and composition of graphene sheets we can create spin-polarized currents in an energy-gapped material. Such an origami-like technique is likely to bring about a whole new range of spintronic features in 2-dimensional systems not possible in 3-dimensional structures.

-
- [1] A. K. Geim, K. S. Novoselov, *Nature Materials* **6**, 183 (2007).
 - [2] K. S. Novoselov, V. I. Falko, L. Colombo, P. R. Gellert, M. G. Schwab and K. Kim, *Nature*, **490** 192 (2012)
 - [3] M. Han et al, *Phys. Rev. Lett.* **98**, 206805 (2007)
 - [4] J. M. Cai et al, *Nature* **466**, 470 (2010)
 - [5] T. Ohta et al, *Science* **313**, 951 (2006)
 - [6] J. B. Oostinga et al, *Nature Mater.* **7**, 151 (2008)
 - [7] V. M. Pereira, A. H. Castro Neto, and N. M. R. Peres, *Phys. Rev. B* **80**, 045401 (2009)
 - [8] Z. H. Ni, T. Yu, Y. H. Lu, Y. Y. Wang, Y. P. Feng, and Z. X. Shen, *ACS Nano* **2**, 2301 (2008)
 - [9] T. M. G. Mohiuddin, A. Lombardo, R. R. Nair, A. Bonetti, G. Savini, R. Jalil, N. Bonini, D. M. Basko, C. Galiotis, N. Marzari, K. S. Novoselov, A. K. Geim, and A. C. Ferrari, *Phys. Rev. B* **79**, 205433 (2009).
 - [10] D. C. Elias et al, *Science* **323**, 610 (2009)
 - [11] K. P. Loh et al, *J. Mater. Chem.* **20**, 2277 (2010)
 - [12] D. Huertas-Hernando, F. Guinea and A. Brataas, *Phys. Rev. B* **74**, 155426 (2006)
 - [13] D. Huertas-Hernando, F. Guinea, and A. Brataas, *Phys. Rev. Lett.* **103**, 146801 (2009)
 - [14] F. S. M. Guimaraes, D. F. Kirwan, A. T. Costa, R. B. Muniz, D. L. Mills and M. S. Ferreira, *Phys. Rev. B* **81**, 153408 (2010)
 - [15] F. S. M. Guimaraes, A. T. Costa, R. B. Muniz and M. S. Ferreira, *Phys. Rev. B* **81**, 233402

(2010)

- [16] N. Tombros, C. Jozsa, M. Popinciuc, H. T. Jonkman, and B. J. van Wees, *Nature* **448**, 571 (2007).
- [17] D. Pesin and A. H. MacDonald, *Nature Mater.* **11**, 409 (2012) and references therein
- [18] W. Han, J. Chen, D. Wang, K. M. McCreary, H. Wen, A. G. Swartz, J. Shi, and R. K. Kawakami, *Nano Lett.* **12**, 3443 (2012); K. M. McCreary, A. G. Swartz, W. Han, J. Fabian, and R. K. Kawakami, *Phys. Rev. Lett.* **109**, 186604 (2012).
- [19] J. Balakrishnan, G. K. W. Koon, M. Jaiswal, A. H. Castro Neto, and Barbaros Özyilmaz, *Nature Phys.* Advance Online Publication, doi:10.1038/nphys2576 (2013).
- [20] A. H. Castro Neto and F. Guinea, *Phys. Rev. Lett.* **103**, 026804 (2009)
- [21] D. Ma, Z. Li and Z. Yang, *Carbon* **50**, 297 (2012)
- [22] C. L. Kane and E. J. Mele, *Phys. Rev. Lett.* **95**, 226801 (2005)
- [23] Y. S. Dedkov, M. Fonin, U. Rudiger and C. Laubschat, *Phys. Rev. Lett.* **100**, 107602 (2008)
- [24] O. Rader et al, *Phys. Rev. Lett.* **102** 057602 (2009)
- [25] J. Hicks et al, *Nature Phys.* **9**, 49 (2013)
- [26] S. R. Power and M. S. Ferreira, *Phys. Rev. B* **83**, 155432 (2011)
- [27] D. Griffiths and S. Walborn, *Am. J. Phys.* **67**, 446 (1999)
- [28] J. V. Gomes and N. M. R. Peres, *J. Phys. Condens. Matter* **20**, 325221 (2008)
- [29] S. M. Avdoshenko, P. Koskinen, H. Sevincli, A. Popov, C. G. Rocha, arXiv:1301.2226

Acknowledgments

MSF acknowledges financial support from Science Foundation Ireland under Grant Number SFI 11/RFP.1/MTR/3083. AHCN acknowledges DOE grant DE-FG02-08ER46512, ONR grant MURI N00014-09-1-1063, and the NRF-CRP award "Novel 2D materials with tailored properties: beyond graphene" (R-144-000-295-281). A. T. C. acknowledges partial financial support from CNPq (Brazil) and INCT Nanomateriais de Carbono.

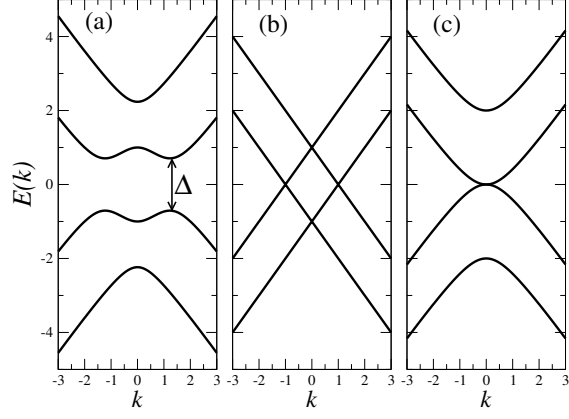


FIG. 1: Dispersion relation $E(k)$ obtained from the four eigenvalues of the Hamiltonian H . (a) In general the electronic structure displays a distinctive bandgap Δ , depicted by the vertical arrow. The energy gap disappears when (b) $\gamma \neq 0$; $\lambda = 0$ or (c) $\gamma = 0$; $\lambda \neq 0$

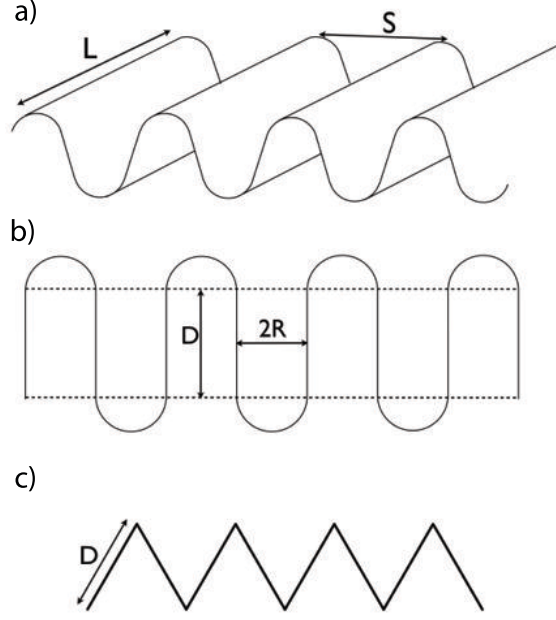


FIG. 2: Schematic diagrams of the corrugated geometry adopted by our graphene sheets. (a) Characteristic shape of corrugated sheets of graphene of width L with a periodicity S . For practical purposes we assume $L \rightarrow \infty$. (b) Cross section of the corrugated graphene sheet used in our calculations, whereby sections of curved graphene with curvature radius R and width πR are spaced by flat regions of width D . For distinction, these two different regions are separated by the horizontal dashed lines. (c) In the limit $R \rightarrow 0$, the corrugated sheet becomes a series of equally spaced sharp creases separated by flat sections of graphene.

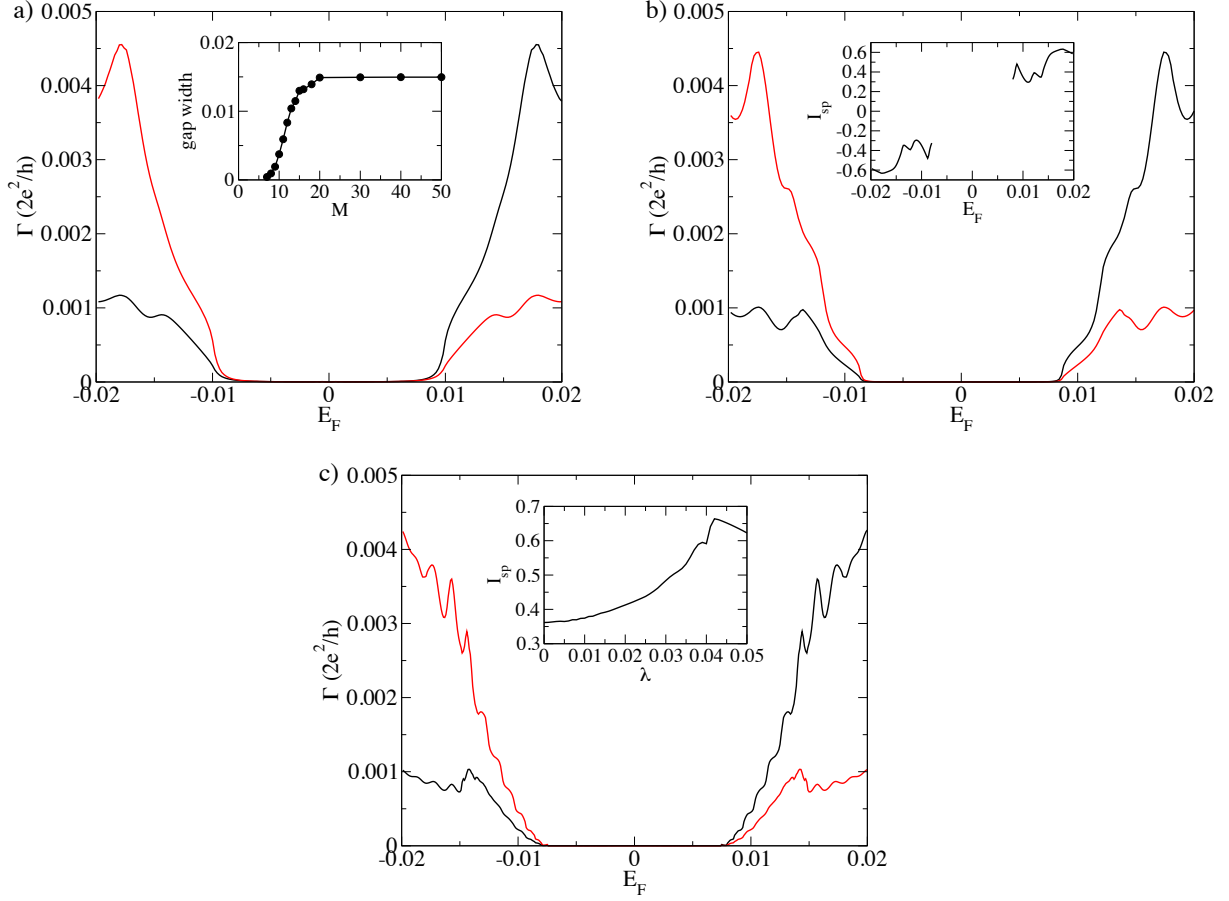


FIG. 3: Spin-dependent conductances of a corrugated sheet made of M curved regions of radius $R \sim 6\text{\AA}$ separated by flat sections of graphene of width $D = 20$. Except for the insets, black (red) lines represent \uparrow (\downarrow) spin-polarized conductances. (a) $M = 10$; $\delta = 5 \times 10^{-2}$; $\lambda = 5 \times 10^{-2}$. The inset shows how the conductance gap scales with M . Note that it tends to a saturation value when $M \gg 1$. (b) $M = 15$; $\delta = 5 \times 10^{-2}$; $\lambda = 5 \times 10^{-2}$. The inset depicts the spin polarization of the current I_{sp} as a function of E_F . Only results outside the bandgap are shown. (c) $M = 50$; $\delta = 5 \times 10^{-2}$; $\lambda = 5 \times 10^{-2}$. Shown in the inset is the dependence of I_{sp} on the SOI parameter λ .

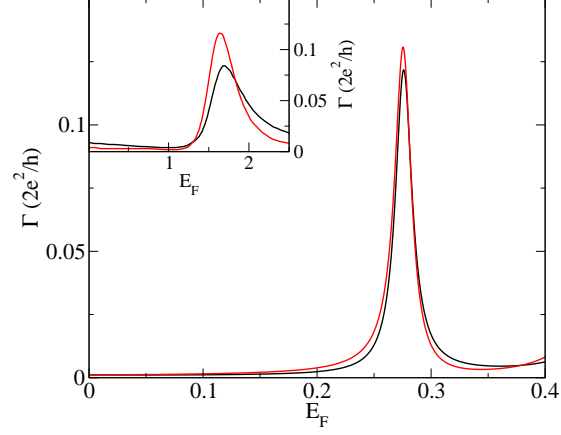


FIG. 4: Electronic transport calculations on creased graphene sheets represented schematically by Fig. 2(c). Spin-dependent conductance results for $M = 2$ delta functions for electrons constrained to move perpendicularly to the creases calculated based on the TB-model (main figure) and on the Continuous model (inset) for $D = a$, a being the lattice parameter of graphene. Black (red) lines represent \uparrow (\downarrow) spin-polarized conductances.